

Metal-rich carbon stars in the Sagittarius Dwarf Spheroidal galaxy

Eric Lagadec¹*, Albert A. Zijlstra¹, G.C. Sloan², Peter R. Wood³, Mikako Matsuura^{4,5}, Jeronimo Bernard-Salas², J.A.D.L. Blommaert⁶, M.-R. L. Cioni⁷, M.W Feast^{8,11}, M.A.T. Groenewegen⁹, Sacha Hony¹⁰, J.W. Menzies¹¹, J.Th. van Loon¹², P.A. Whitelock^{8,11,13}

¹Jodrell Bank Centre for Astrophysics, The University of Manchester, School of Physics & Astronomy, Manchester M13 9PL, UK

²Department of Astronomy, Cornell University, 108 Space Sciences Building, Ithaca NY 14853-6801, USA

³Research School of Astronomy and Astrophysics, Australian National University, Cotter Road, Weston Creek, ACT 2611, Australia

⁴Division of Optical and IR Astronomy, National Astronomical Observatory of Japan, Osawa 2-21-1, Mitaka, Tokyo 181-8588, Japan

⁵Department of Physics and Astronomy, University College London, Gower Street, London WC1E 6BT, UK

⁶Instituut voor Sterrenkunde, K.U.Leuven, Celestijnenlaan 200D, 3001 Leuven, Belgium

⁷Centre for Astrophysics Research, University of Hertfordshire, Hatfield AL10 9AB, UK

⁸Astronomy Department, University of Cape Town, 7701, Rondebosch, South Africa

⁹Koninklijke Sterrenwacht van België, Ringlaan 3, 1180 Brussels, Belgium

¹⁰CEA, DSM, DAPNIA, Service d'Astrophysique, CEA Saclay, 91191 Gif-sur-Yvette Cedex, France

¹¹South African Astronomical Observatory, PO Box 9, 7935 Observatory, South Africa

¹²Astrophysics Group, School of Physical & Geographical Sciences, Keele University, Staffordshire ST5 5BG, UK

¹³National Astrophysics and Space Science Programme, Department of Mathematics and Applied Mathematics University of Cape Town, 7701 Rondebosch, South Africa

Accepted . Received

ABSTRACT

We present spectroscopic observations from the *Spitzer Space Telescope* of six carbon-rich AGB stars in the Sagittarius Dwarf Spheroidal Galaxy (Sgr dSph) and two foreground Galactic carbon stars. The band strengths of the observed C_2H_2 and SiC features are very similar to those observed in Galactic AGB stars. The metallicities are estimated from an empirical relation between the acetylene optical depth and the strength of the SiC feature. The metallicities are higher than those of the LMC, and close to Galactic values. While the high metallicity could imply an age of around 1 Gyr, for the dusty AGB stars, the pulsation periods suggest ages in excess of 2 or 3 Gyr. We fit the spectra of the observed stars using the DUSTY radiative transfer model and determine their dust mass-loss rates to be in the range $1.0\text{--}3.3 \times 10^{-8} M_{\odot} \text{yr}^{-1}$. The two Galactic foreground carbon-rich AGB stars are located at the far side of the solar circle, beyond the Galactic Centre. One of these two stars show the strongest SiC feature in our present Local Group sample.

Key words: circumstellar matter — stars: carbon — stars:AGB and post-AGB — stars: mass loss — galaxies: individual: Sagittarius dwarf Spheroidal — infrared: stars

1 INTRODUCTION

The Asymptotic Giant Branch (AGB) phase occurs during the late stages of the evolution of low- and intermediate-mass stars. This phase is characterised by intense mass loss and leads to the formation of a circumstellar envelope made of gas and dust. The molecular composition of this envelope is dependent on the C/O abundance ratio. The CO molecule is very stable and unreactive, and if $C/O > 1$, all the oxygen is trapped in CO. The envelope (and

star) is then “carbon-rich”; amorphous carbon dominates the dust, while (after H_2) CO and C_2H_2 dominate its gas. The “oxygen-rich” AGB stars are characterised by silicate dust and molecules such as SiO, OH, H_2O . Third dredge-up brings the carbon produced by the triple- α reactions to the surface, increasing the C/O ratio and over time can change a star from oxygen-rich to carbon-rich.

The mass loss from AGB stars is one of the main agents for the chemical evolution of galaxies. It expels the products of nuclear reactions in the core of the star into the interstellar medium. The mass loss from AGB stars contributes roughly half of all the gas recycled by stars (Maeder 1992), and up to nearly 90% of the dust

* E-mail: eric.lagadec@manchester.ac.uk

(Gehrz 1989). Mass loss from AGB stars is also one of the main sources of carbon in the universe, together with Wolf-Rayet stars and supernovae (Dray et al. 2003).

The mechanisms driving this mass-loss process are not fully understood. It is thought to be a two-step process: pulsations from the star lead to the formation of dust, and then radiation pressure accelerates the dust grains to the escape velocity. The gas is then also expelled due to friction with the dust grains. The effect of metallicity on the mass-loss rates from AGB stars has been discussed at some length. Some works proposed that mass-loss rates should be lower in metal-poor environments, as less dust is expected to form, so that radiation pressure would be less efficient in driving the mass loss (Bowen & Willson 1991; Zijlstra 2004). This hypothesis on the metallicity effect on mass loss has recently been tested using spectroscopy from *Spitzer* (e.g. Sloan et al. 2006, 2008; Zijlstra et al. 2006b; Lagadec et al. 2007; Matsuura et al. 2007; hereafter “SZLM” will refer to all five of these papers). Against early expectations, the dust mass-loss rates of carbon stars in metal-poor galaxies from the Local Group appear to be similar to the ones measured in the Galaxy. In contrast, oxygen-rich stars in metal-poor environments do appear to have lower dust mass-loss rates. This suggests that carbon is important in triggering the superwind (Lagadec & Zijlstra 2008). Theoretical models confirm that the mass-loss rates of carbon stars should not depend on metallicity (Wachter et al. 2008). Mattson et al. (2008) argue that the pulsation energy of the star can drive a strong wind at low metallicity, but the dependence on chemistry suggests this is not the dominant effect within the observed metallicity range.

The dusty circumstellar envelope surrounding AGB stars absorbs the light from the central star and re-emits it in the infrared. Furthermore, spectral signatures of dust and molecules appear in this wavelength range. Spectroscopic observations of AGB stars in the thermal infrared are therefore vital for the study of the dusty envelopes around these stars. Atmospheric absorption prevents ground-based mid-infrared observations outside two windows around 10 and 20 μm . The *Spitzer Space Telescope* (Werner et al. 2004), with its high sensitivity and mid-infrared wavelength coverage, has proven to be a valuable tool for the study of dusty envelopes around extragalactic AGB stars.

To study the mass loss from evolved stars at low metallicity, we are undertaking a *Spitzer* spectroscopic survey of mass-losing AGB stars in different Local Group galaxies. We have already presented results for the Magellanic Clouds and Fornax (SZLM; Matsuura et al. 2006; Groenewegen et al. 2007). Here we present *Spitzer* spectra of eight AGB stars in the direction of the Sagittarius Dwarf Spheroidal (Sgr dSph) galaxy.¹ This study aims at studying the circumstellar properties of these AGB stars.

2 TARGET SELECTION

We selected eight AGB candidates in the direction of the Sgr dSph based on their near-infrared colours. These stars were not spectroscopically confirmed carbon stars before this study. The core of the Sgr dSph has a distance modulus estimated to be 17.02 ± 0.19 (Mateo et al. 1995) and is located behind the Galactic Bulge. It is being disrupted by the Galaxy so that its tidal tail surrounds the Milky Way. It contains several stellar populations. The dominant

¹ This galaxy is also known as the Sagittarius Dwarf Elliptical Galaxy (SagDEG), but it should not be confused with the Sagittarius Dwarf Irregular Galaxy (SagDIG).

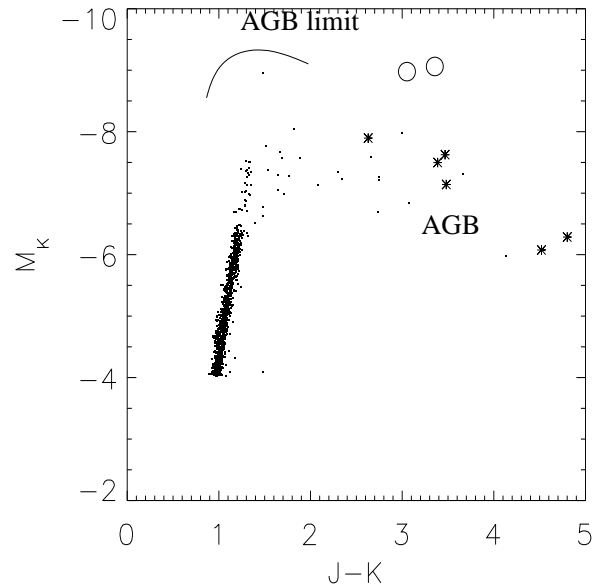


Figure 1. The M_K vs $J - K$ diagram of the observed sample. Crosses represent the observed Sgr dSph targets and the large circle the foreground targets. Points represent the stellar population of Sgr dSph. M_K is the absolute magnitude and was calculated assuming a distance modulus estimated to be 17.02 ± 0.19 (Mateo et al. 1995).

one has a metallicity in the range $[\text{Fe}/\text{H}] = -0.4$ to -0.7 and an age of 8.0 ± 1.5 Gyr (Bellazzini et al. 2006). A second population is younger and more metal-rich with $[\text{Fe}/\text{H}] = -0.25$ for the most metal-rich objects (Zijlstra et al. 2006a). These populations span the range of metallicities observed in the Magellanic Clouds.

The eight selected targets are a subsample of the stars presented by Lagadec et al. (2008). Table 1 lists some characteristics of these stars. For convenience, we will use the names published previously. The stars were selected to span a wide range in $J - K$ colour, i.e. a wide range of optical depth due to dust in their envelopes.

Fig. 1 displays the eight observed stars in an M_K vs $J - K$ diagram. Asterisks represent the observed stars in the Sgr dSph. To show that the observed stars are all AGB stars, we overplot the distribution of Sgr field stars. Lagadec & Zijlstra (2008) explain the selection of these field stars. To verify that the observed stars belong to Sgr dSph, we performed radial velocity measurements: these indicate that six out of the eight observed stars belong to Sgr dSph but the remaining two are foreground stars (see Sec. 3.3).

3 OBSERVATIONS AND DATA REDUCTION

3.1 *Spitzer* observations

The observations were made with the InfraRed Spectrograph (IRS, Houck et al. 2004), on board the *Spitzer Space Telescope*. We used the Short-Low (SL) and Long-Low (LL) modules to cover the wavelength range 5–38 μm . The SL and LL modules are each divided in two spectral segments, together known as SL2, SL1, LL2 and LL1; a “bonus” order covering the overlap between the two modules is also available. The data reduction is similar to that described by Zijlstra et al. (2006b). The raw spectra were processed

through the *Spitzer* pipeline S15. We replaced the bad pixels by values estimated from neighbouring pixels. The sky was subtracted by differencing images aperture by aperture in SL and nod by nod in LL. We used the software tools available in SPICE (the *Spitzer* IRS Custom Extractor) to extract the spectra. The flux calibration made use of the reference stars HR 6348 (K0 III) in SL and HR 6348, HD 166780 (K4 III) and HD 173511 (K5 III) in LL. The spectra were individually extracted from the individual images. Both nods in both apertures were then joined simultaneously, recalculating the errors in the process by comparing the nods. The different nods were averaged, using the differences to estimate the errors. The different spectral segments were combined using scalar multiplication to eliminate the discontinuities due to flux lost because of pointing errors. The different segments were also trimmed to remove dubious data at their edges. We also retained the data in the bonus order where it was valid. These steps resulted in a standard wavelength calibration accuracy of $0.06 \mu\text{m}$ in SL and $0.15 \mu\text{m}$ in LL.

Fig. 2 presents the spectra of the observed AGB stars, ordered by their [6.4]-[9.3] colours (see Sec. 5). The molecular bands and dust features discussed below identify all eight objects as carbon-rich stars.

3.2 Near-infrared photometry

Observations in the near-infrared are important to obtain a reliable estimate of the luminosity. Due to the variability, these observations are best obtained close to the same epoch as the spectra. Multi-epoch *JHKL* photometry was obtained at the Australian National University (ANU) 2.3-m telescope at Siding Spring Observatory (SSO) in Australia. The filters used were centred at $1.28 \mu\text{m}$ (*J*), $1.68 \mu\text{m}$ (*H*), $2.22 \mu\text{m}$ (*K*) and $3.59 \mu\text{m}$ (*L*). Groenewegen et al. (2007) describe the observations. Table 1 presents the measured *JHKL* magnitudes at the epoch of the *Spitzer* observations.

The multi-epoch observations, taken before the *Spitzer* observations, were used to study the near-infrared variability of the sources. Light curves were obtained by fitting a sine wave to the *K*-band data. Fig. 3 displays these light curves.

3.3 Radial velocities

Radial velocities were determined for six of the eight carbon stars using optical spectra obtained with the Dual Beam Spectrograph on the 2.3-m SSO telescope. The spectra have a resolution of $0.48 \text{ \AA}/\text{pixel}$ for four objects and $3.7 \text{ \AA}/\text{pixel}$ for the remaining two objects (see Table 2). The higher resolution spectra were cross-correlated with the local carbon star X Vel for which a spectrum at a resolution of $0.5 \text{ \AA}/\text{pixel}$ was also obtained. A radial velocity of -5.4 km s^{-1} was adopted for X Vel (determined from high-resolution echelle spectra which were cross correlated against the radial velocity standard α Cet with a heliocentric radial velocity of -25.8 km s^{-1}). Cross-correlation of the lower-resolution spectra of the remaining two stars was used to obtain their radial velocities. Table 2 gives the final heliocentric radial velocities and their errors (as given by the IRAF task FXCOR).

Fig. 4 presents a histogram of the radial velocities of carbon stars in the direction of Sgr dSph from Ibata et al. (1997). There are obviously two groups of stars: those with heliocentric radial velocities of $100 < v_{\text{helio}}(\text{km/s}) < 190$ which belong to the Sgr dSph; and those with $v_{\text{helio}}(\text{km/s}) < 50$ which belong to the Milky Way Galaxy. Two stars in our sample, Sgr 02 and Sgr 22, clearly

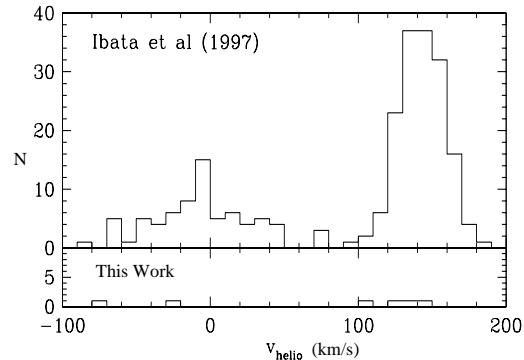


Figure 4. Top panel: Radial velocity distribution of stars in the direction of the Sgr dSph galaxy (from Ibata et al. 1997). Bottom panel: radial velocity distribution of six of our targets. Two of these stars, Sgr 02 and Sgr 22, are clearly foreground members of the Galaxy.

Table 2. Heliocentric radial velocities for six of the observed targets as measured from observations at SSO.

Target	Resolution $\text{\AA}/\text{pixel}$	wavelength range \AA	v_{helio} km/s	v_{error} km/s
Sgr 02	0.48	8100-8900	-22.8	1.1
Sgr 03	3.7	6800-9200	128.1	11.1
Sgr 09	0.48	8100-8900	144.9	1.6
Sgr 15	3.7	6800-9200	136.4	12.2
Sgr 22	0.48	8100-8900	-73.1	2.1
Sgr 29	0.48	8100-8900	106.3	2.5

belong to the Milky Way Galaxy, while the other stars are members of the Sgr dSph. The properties of the two foreground stars are discussed in Sec. 9.3

We used other distance estimates to ascertain the Sgr dSph membership of the two stars without radial velocity measurements (see Sec. 7).

4 DESCRIPTION OF THE SPECTRA

The IRS spectra of the eight observed stars (Fig. 2) show both dust and molecular emission. All the observed stars are carbon-rich and have spectra typical of AGB stars. The spectra of all stars clearly show absorption features from C_2H_2 at 7.5 and $13.7 \mu\text{m}$ (Fig. 5). SiC dust produces the $11.3 \mu\text{m}$ feature detected in all the spectra. Some of them (Sgr 02, Sgr 03, Sgr 07 and Sgr 18) show a broad emission feature around $30 \mu\text{m}$ attributed to MgS (Hony et al., 2002). This feature might also be present in Sgr 09 and Sgr 22. A drop is observed for all stars at the blue edge of the spectra. It is due to several molecules, most notably C_3 and CO (Zijlstra et al. 2006b).

Sgr 22 displays a very strong SiC emission feature, stronger than any carbon-rich AGB star of which we are aware, including the Galactic sample observed by the *Infrared Space Observatory* and described by Sloan et al. (2006) or the Local Group galaxies observed by *Spitzer* (see upper panel of Fig. 8).

A weak feature attributed to the stretching vibration of a carbonyl group (X-CO) has been observed in some LMC AGB stars

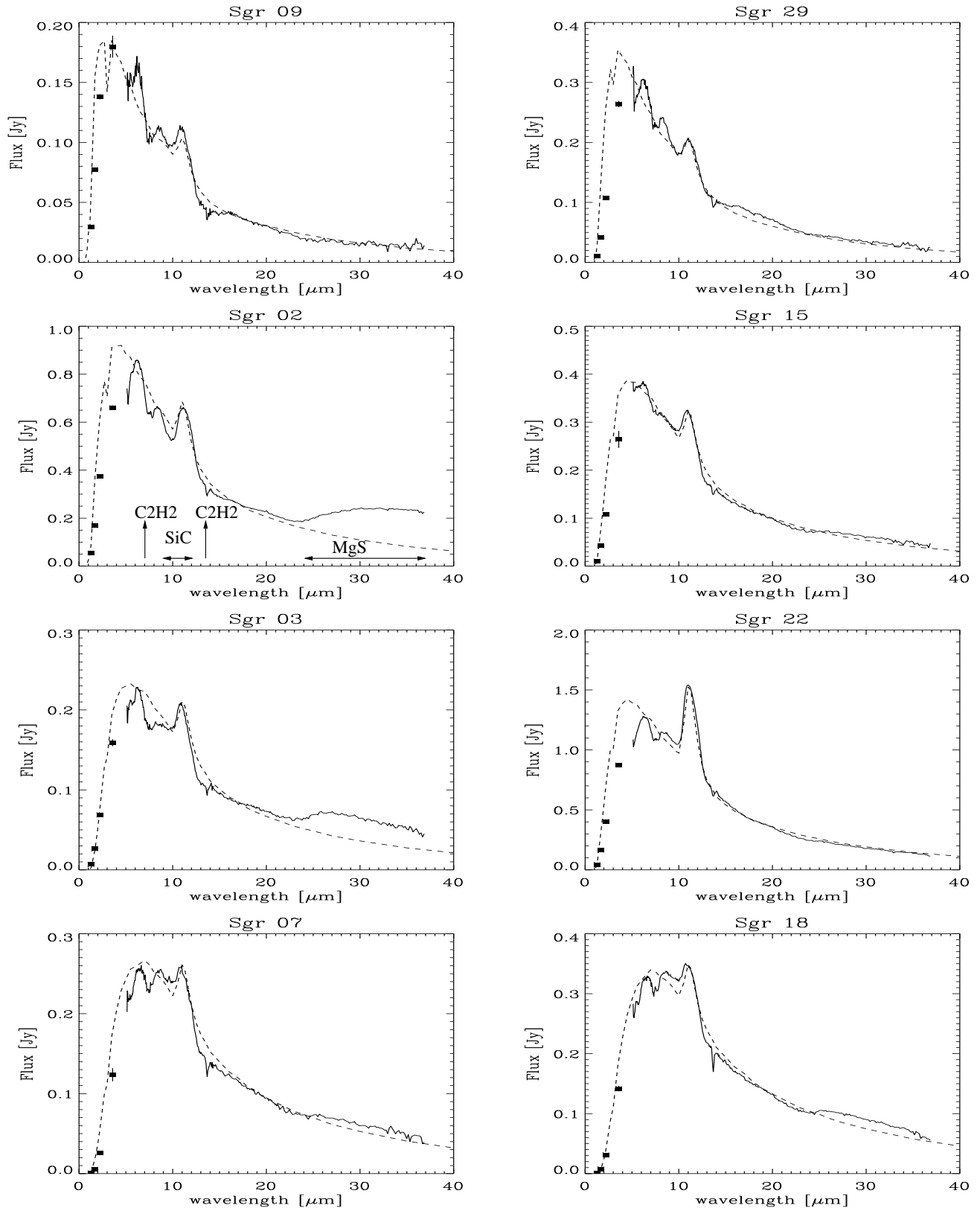


Figure 2. Spitzer/IRS spectra of the eight observed carbon stars, ordered by dust temperature. The main dust and gas features are labelled on the spectrum of Sgr 02. The dashed lines represent the SED fits obtained with DUSTY (Sec. 8)

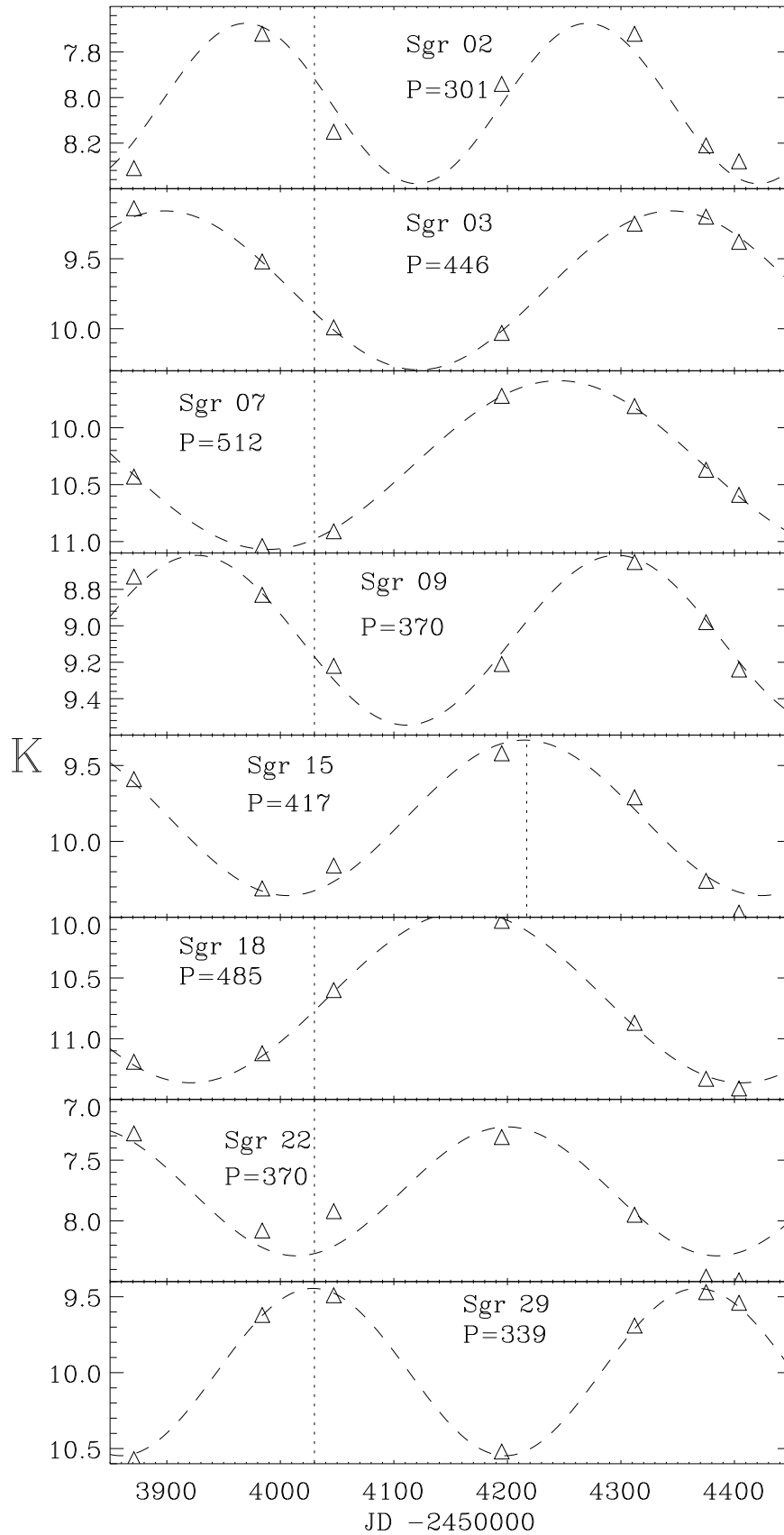


Figure 3. Light curves of the eight observed carbon stars. These were obtained using a sinusoidal fit to the *K*-band magnitudes. The vertical lines show the dates of our *Spitzer* observations.

Table 1. Observed Sgr dSph targets: adopted names, coordinates, photometry and distance. *J*, *H*, *K* and *L* are taken from near-simultaneous measurements at SSO. The periods were obtained by sine-fit to the *K*-band observations. The distance was estimated using the method described in Sec. 7.

Adopted name	2MASS name	IRAS name	RA	Dec (J2000)	<i>J</i> mag	<i>H</i> mag	<i>K</i> mag	<i>L</i> mag	<i>P</i> d	phase	D kpc
Sgr02	18414350–3307166	18384–3310	18 41 43.50	–33 07 16.6	11.095	9.421	8.043	6.501	301	0.65	17.1
Sgr03	18443095–3037098	18413–3040	18 44 30.96	–30 37 09.8	13.360	11.436	9.879	8.047	446	0.36	31.6
Sgr07	18465160–2845489	18436–2849	18 46 51.60	–28 45 48.9	15.464	13.121	10.944	8.320	512	0.06	34.1
Sgr09	18514105–3003377		18 51 41.05	–30 03 37.7	11.753	10.263	9.124	7.913	370	0.40	30.3
Sgr15	18584385–2956551	18555–3001	18 58 43.85	–29 56 55.1	12.862	10.921	9.394	7.496	417	1.00	28.0
Sgr18	19043562–3112564	19013–3117	19 04 35.62	–31 12 56.4	15.535	12.753	10.734	8.171	485	0.42	35.1
Sgr22	19103987–3228373	19074–3233	19 10 39.87	–32 28 37.3	11.315	9.454	7.959	6.196	370	0.02	16.0
Sgr29	19485065–3058317		19 48 50.65	–30 58 31.9	12.909	11.014	9.522	7.838	339	1.00	31.5

(Zijlstra et al. 2006b) at $5.8\mu\text{m}$. This feature is present in the spectra of Sgr09 and Sgr18, and possibly also in Sgr02, Sgr03, Sgr07 and Sgr15.

5 COLOURS AND BAND STRENGTHS

To determine colours of the observed stars, we applied the so-called “Manchester System” (Sloan et al. 2006; Zijlstra et al. 2006b), using four narrow bands selected to represent the continuum at different wavelengths. Using this method, we derive two colours. Zijlstra et al. (2006b) showed that the [6.4]–[9.3] colour is a good estimate of the dust optical depth, while the [16.5]–[21.5] colour provides an estimate of the dust temperature. The [6.4]–[9.3] colour shows a linear relation with the measured mass-loss rates (Groenewegen et al. 2007; Matsuura et al. 2007; Sloan et al. 2008). Table 3 lists the blackbody temperature derived from this [16.5]–[21.5] colour. To test that our choice of continuum colours is reasonable, we plotted [16.5]–[21.5] vs. [6.4]–[9.3] (Fig. 6). For five of the observed stars, the continua are consistent. But three stars (Sgr02, Sgr03 and Sgr22) are outliers. Sgr02, Sgr03 are particularly red at [16.5]–[21.5].

For all the observed stars, we measured the strength of the main features (Fig. 2). The continuum underlying each feature is defined using small wavelength ranges on the blue and red sides of the feature. The continuum is then defined using a straight line between the blue and red continuum values. Because the red edge of the MgS feature (Sec. 4) is outside of the IRS spectral range, we used a blackbody with the temperature derived from the [16.5]–[21.5] to extrapolate the continuum under this dust feature. After the definition of the continuum we determined the strengths of the features in two different ways. For the dust features, we simply measured the ratio between the integrated feature flux and the continuum (*F/C*). For the gas features, seen in absorption, we measured the equivalent widths. We also measured the central wavelength of the SiC feature defined as the wavelength at which the flux on the blue side of the feature equals the flux on the red side. Table 3 lists the measured strengths and central wavelengths of the observed features.

6 CIRCUMSTELLAR PROPERTIES

6.1 Gas

As mentioned in Sec. 4, the main gas absorption features observed in our spectra at $7.5\mu\text{m}$ and $13.7\mu\text{m}$ are due to C_2H_2 . We have shown (SZLM, Matsuura et al. 2006) that in metal-poor environments, the C_2H_2 absorption becomes stronger. This can be explained by the fact that at low metallicity, the initial oxygen abundance is smaller than for Galactic stars, and the dredge-up of carbon during the AGB leads to higher C/O ratios.

Fig. 7 shows the equivalent width of these features as a function of the [6.4]–[9.3] colour for the current sample in comparison to the stars from other Local Group galaxies. The plot relates the strength of the molecular band to the optical depth (or dust mass-loss rates) of the envelopes of the observed stars. The C_2H_2 equivalent widths of the Sgr dSph sample are in the lower range of the observed strengths. They are similar to or a little higher than the values found in Galactic stars of similar [6.4]–[9.3], but are generally weaker than found in the SMC, LMC and Fornax.

6.2 Dust

As mentioned in Sec. 4, the main dust features observed in the spectra are due to SiC and MgS. The featureless continuum arises primarily from emission from amorphous carbon emission. Fig. 8 shows the strength of the SiC and MgS features as a function of the [6.4]–[9.3] colour.

The properties of the SiC feature have been extensively studied previously (e.g. Speck et al. 2005, Leisenring et al. 2008). Lagadec et al. (2007) have shown that the relationship between the strength of the SiC feature and the optical depth of the envelope varies according to the metallicity of the host galaxy, using a sample of stars in the SMC, LMC and the Galaxy. Fig. 8 illustrates the trend of increasing SiC feature strength for the Galactic stars when [6.4]–[9.3] $\lesssim 0.5$ and a gradual decrease for redder stars. Such a trend is observed for carbon stars in the LMC, but the inflexion occurs for redder colours, around ~ 1 . Very few SMC and Fornax stars with [6.4]–[9.3] > 1 have been observed, but such stars in metal-poor galaxies appear to follow the same trend as LMC stars and have much weaker SiC features at a given optical depth. One SMC star, GM 780, is an outlier with a very strong SiC emission feature. The stars from the Sgr dSph are located at similar positions as the Galactic ones, but with a SiC feature slightly weaker than those of Galactic stars with the same [6.4]–[9.3] colour. As Si is not

Table 3. Colours measured using four narrow carbon stars continuum bands, strength of the molecular and dust features, in terms of either the equivalent width in microns, or the integrated flux-to-continuum ratio, F/C (Sect. 5). The last column gives the continuum (black-body) temperature, derived from the [16.5]–[21.5] colour listed in Table 1

target	[6.4]–[9.3] (mag)	[16.5]–[21.5] (mag)	EW (7.5 μ m) (μ m)	EW (13.7 μ m) (μ m)	F/C(SiC)	λ_c (SiC) (μ m)	F/C (MgS)	T(K)
Sgr 02	0.375 \pm 0.012	0.270 \pm 0.010	0.148 \pm 0.002	0.035 \pm 0.005	0.267 \pm 0.005	11.27 \pm 0.03	0.639 \pm 0.012	515. \pm 16.
Sgr 03	0.555 \pm 0.004	0.292 \pm 0.009	0.115 \pm 0.005	0.020 \pm 0.008	0.226 \pm 0.007	11.07 \pm 0.05	0.401 \pm 0.012	480. \pm 12.
Sgr 07	0.757 \pm 0.004	0.187 \pm 0.015	0.078 \pm 0.005	0.036 \pm 0.002	0.157 \pm 0.004	11.17 \pm 0.04	0.180 \pm 0.018	716. \pm 48.
Sgr 09	0.319 \pm 0.016	0.093 \pm 0.018	0.237 \pm 0.009	0.064 \pm 0.011	0.278 \pm 0.008	11.14 \pm 0.04	0.050 \pm 0.026	1385. \pm 225.
Sgr 15	0.532 \pm 0.006	0.152 \pm 0.014	0.061 \pm 0.004	0.018 \pm 0.005	0.222 \pm 0.005	11.11 \pm 0.03	0.172 \pm 0.018	864. \pm 66.
Sgr 18	0.821 \pm 0.002	0.188 \pm 0.013	0.068 \pm 0.004	0.034 \pm 0.003	0.158 \pm 0.003	11.18 \pm 0.03	0.234 \pm 0.015	710. \pm 41.
Sgr 22	0.636 \pm 0.005	0.089 \pm 0.016	0.093 \pm 0.002	0.023 \pm 0.002	0.410 \pm 0.006	11.20 \pm 0.02	0.055 \pm 0.020	1457. \pm 225.
Sgr 29	0.362 \pm 0.010	0.105 \pm 0.017	0.131 \pm 0.004	0.044 \pm 0.010	0.189 \pm 0.008	11.22 \pm 0.06	0.001 \pm 0.021	1230. \pm 166.

produced in AGB stars, this slight difference appears to indicate that the Si abundance in the observed Sgr dSph stars is between the Si abundance of Fornax/SMC/LMC and the Galaxy.

Fig. 9 shows the strength of the MgS feature as a function of the dust temperature. As already observed for AGB stars in other Local Group galaxies (Sloan et al. 2006, Zijlstra et al. 2006b, Lagadec et al. 2007), this feature tends to appear mostly in the envelopes of stars with cool dust. In general, the formation process of MgS begins around 600 K and is complete around 300 K.

7 DISTANCE ESTIMATES

To check whether the observed stars are members of Sgr dSph, we estimated their distances using two methods. The distance to Sgr dSph being well established, our sample allows us to test different distance estimation methods.

The first one uses the infrared colours of the observed stars, following the method described by Sloan et al. (2008). They have shown, from a sample of carbon stars in the Magellanic Clouds, that:

$$M_K = -9.18 + 0.395(J - K) \quad (1)$$

and

$$M_{9.3\mu m} = \sum a_i ([6.4] - [9.3])^i \quad (2)$$

where $a_0 = -8.81$, $a_1 = -6.56$ and $a_2 = 2.74$. Using these relations and the infrared colours of the observed carbon stars, we can obtain two estimates of their distances.

The second method makes use of the period-luminosity relation for carbon Miras as described by Feast et al. (2006):

$$M_{bol} = -2.54 \times \log P + 2.06 \quad (3)$$

We converted all of the photometry to the SAAO system and dereddened the near-infrared data as described by Lagadec et al. (2008). The reddening was estimated using the extinction maps by Schlegel et al. (1998). For the observed stars, $A_J \sim 0.1$ and $A_K \sim 0.04$. Using standard conversion factors, we estimated that $A_{6\mu m} < 0.01$ and that the reddening was lower than a percent at longer wavelengths. We thus did not deredden our spectra. We then derived the bolometric magnitudes using the equation for bolometric correction derived by Whitelock et al. (2006):

$$BC_K = +0.972 + 2.9292 \times (J - K) - 1.1144 \times (J - K)^2$$

Table 4. Distances estimated from the infrared colours and the period-luminosity relation.

target	D_{IR} (kpc)	D_{PL} (kpc)
Sgr 02	17.1	12.9
Sgr 03	31.6	33.2
Sgr 07	34.1	41.4
Sgr 09	30.3	25.2
Sgr 15	28.0	25.8
Sgr 18	35.1	32.7
Sgr 22	16.0	12.9
Sgr 29	31.5	25.1

$$+0.1595 \times (J - K)^3 - 9.5689 \text{ } 103(J - K)^4 \quad (4)$$

Table 4 displays the mean values of the estimated distance for each star using the dereddened infrared colours and the period-luminosity relation. This confirms that the stars Sgr 07 and Sgr 18 belong to Sgr dSph.

Mateo et al. (1995) derived a distance for the central region of Sgr dSph of 25.35 ± 2.06 kpc. A comparison of our two distance estimates indicates that the best agreement with the distance to Sgr dSph is obtained with the period-luminosity relation. Using the infrared colours gives distances to the observed stars significantly higher than the well-determined distance to the galaxy. The distance estimated using the period-luminosity relation gives results in perfect agreement for Sgr 09, Sgr 15 and Sgr 29. For the three other stars, this method gives larger distances. Variability will have some effect on the derived distances, but given that two of the three stars with large apparent distances are significantly redder in $J - K$ than any of the others it would seem quite possible that they are undergoing obscuration events of the type described by Whitelock et al. (2006) for Galactic Miras and which are also seen in at least one of the AGB stars in Fornax (Whitelock et al. 2009). Photometric monitoring over long time scales of these stars would be needed to confirm that hypothesis, as stars with such behaviours show variations over periods of a few years.

8 DUST MASS-LOSS RATES

Lagadec et al. (2008) measured the dust mass-loss rates of the stars presented in this work. These dust mass-loss rates (\dot{M}_{col}), mea-

Table 5. Dust mass-loss rates for the observed stars and parameters obtained from our DUSTY models. \dot{M}_{col} and \dot{M}_{dusty} are the dust mass-loss rates (in $M_{\odot}\text{yr}^{-1}$) from Lagadec et al. 2008 and our DUSTY models, respectively.

Target	Luminosity (L_{\odot})	\dot{M}_{DUSTY} ($10^{-8}M_{\odot}\text{yr}^{-1}$)	T_{eff} (K)	T_{in} (K)	SiC/AMC	τ (0.55 μm)	\dot{M}_{col} ($10^{-8}M_{\odot}\text{yr}^{-1}$)	V_{exp} km/s
Sgr 02	11469	2.59	2800	1200	0.1	4.67	0.86	28
Sgr 03	4529	1.29	2800	1200	0.1	9.56	0.84	18
Sgr 07	4483	2.52	2800	1000	0.08	9.64	0.97	14
Sgr 09	6652	1.02	2800	1200	0.1	2.22	0.27	27
Sgr 15	8632	2.73	2800	1200	0.1	7.00	0.93	23
Sgr 18	5056	3.39	2800	1000	0.08	13.1	2.60	13
Sgr 22	13321	3.78	2800	1200	0.2	7.11	1.30	26
Sgr 29	9152	2.04	2800	1500	0.1	5.89	0.96	35

sured from near and mid-infrared colours are presented in Table 5.

The *Spitzer* spectra, together with simultaneous near-infrared photometric measurements give us an opportunity to better model the dust emission from these stars. We modeled the spectral energy distributions (SEDs), defined by the *JHKL* flux and the *Spitzer* spectra, using the radiative transfer code DUSTY (Ivezic & Elitzur 1997). Our primary objective is to fit the dust continuum in order to estimate the optical depths and the mass-loss rates. DUSTY solves the 1-D problem of radiation transport in a dusty environment. For all our models, we assume that the irradiation comes from a point source (the central star) at the centre of a spherical dusty envelope. The circumstellar envelope is filled with material from a radiatively driven wind. All the stars are carbon-rich and display SiC in emission. We thus assumed that the dust composition of the envelope is a mixture of amorphous carbon and SiC. Optical properties for these dust grains are taken from the work of Hanner (1988) and Pegourie (1988) for amorphous carbon and SiC, respectively. The grain-size distribution is assumed to be a typical MRN distribution, with a grain size a varying from 0.0005 to 0.25 μm distributed according to a power law with $n(a) \propto a^{-q}$ with $q=3.5$ (Mathis et al. 1977). The outer radius of the dust shell was set to 10^3 times the inner radius; this parameter has a negligible effect on our models.

To model the emission from the central star, we used a hydrostatic model including molecular opacities (Loidl et al. 2001, Groenewegen et al. 2007). We used those hydrostatic models as an illuminating source only, we did not attempt to model the molecular absorption features. The C/O ratio is assumed to be 1.1 for the hydrostatic models, which is a typical value for Galactic AGB stars. This ratio is not well known in the observed stars: the C/O ratio of AGB stars appears to be higher in metal-poor environments than in the Galaxy (Matsuura et al. 2002, 2005). But varying the C/O ratio mainly affects the depth of the molecular features (such as CO and C₂H₂). The radiative transfer model fits the dust emission, and the C/O ratio has little effect on the model. We also performed some model calculations assuming that the central star emits as a blackbody, but these did not provide satisfactory fit to the near-infrared data, due to the absence of molecular absorption. The free parameters of the models are the dust temperature at the inner radius, the mass ratio of SiC to amorphous carbon dust and the central star effective temperature, T_{eff} . As one output, DUSTY provides an estimate of the terminal outflow velocity and the mass-loss rate for a luminosity of $10^4 L_{\odot}$. As the luminosity can be determined by scaling the emerging spectrum, we can then recalibrate the mass-loss

rates accordingly, assuming a distance of 25 kpc for the six stars in Sgr dSph, and 17.1 and 16.0 kpc for Sgr 02 and Sgr 22 respectively.

DUSTY gives total (gas+dust) mass-loss rates assuming a gas-to-dust ratio of 200, but the dust is the dominant constraint on the fitting to the SED. Therefore, we have divided the resulting mass-loss rates by the gas-to-dust ratio and report only the dust mass-loss rate in Table 5. This assumes that the gas and dust expansion velocities are the same. Note that we had to make a number of assumptions in our models. For example, we assume that the envelope and the dust grains are spherical. This cannot be the case in reality, so our fits cannot be perfect. However, the models achieve our primary aim, estimating the dust mass-loss rates. These values are of the same order of magnitude as those derived by Lagadec et al. (2008). The values found by Lagadec et al. (2008) are generally a factor of two or three smaller than the present ones.

For all the stars, the best fit is obtained with $T_{\text{eff}}=2800\text{K}$. The best model for most of the stars was obtained using a temperature at the inner radius of 1200 K and a mixture of 10% of SiC and 90% of amorphous carbon. For two stars, we needed $T_{\text{in}}=1000\text{K}$ to model the red part of the SED, and for another one we used $T_{\text{in}}=1500\text{K}$. The very strong SiC feature observed in the spectrum of Sgr 22 is very well fitted using 20% of SiC. Sgr 07 and Sgr 18 have weaker SiC features, which can be fitted using a SiC mass fraction of 8%.

We confirm the general correlation found by Groenewegen et al. (2007) and Matsuura et al. (2007) between the mass-loss rates and the [6.4]–[9.3] (Fig 10). But the stars we observed in the Galaxy and in Sgr dSph are on average offset towards higher mass-loss rates for the same colour, by about a factor of two. The two stars in Fornax show a (smaller) offset in the same direction. All of these mass-loss rates of these stars were estimated from our DUSTY models, while the ones in the Magellanic Cloud stars were estimated using another radiative transfer model (Groenewegen et al., 2007). The models by Groenewegen et al. (2007) were made assuming a constant expansion velocity of 10 km s⁻¹ while DUSTY calculates an expansion velocity for each model. These calculated velocities are generally a factor of 2-3 higher than the ones assumed by Groenewegen et al., suggesting that the difference in mass-loss rates arise from different assumptions made by the models, rather than an intrinsic difference between the stars. The dust mass-loss rates determined by Lagadec et al. (2008) for the Sgr dSph stars nicely follow the relation with [6.4]–[9.3] colour found in previous work.

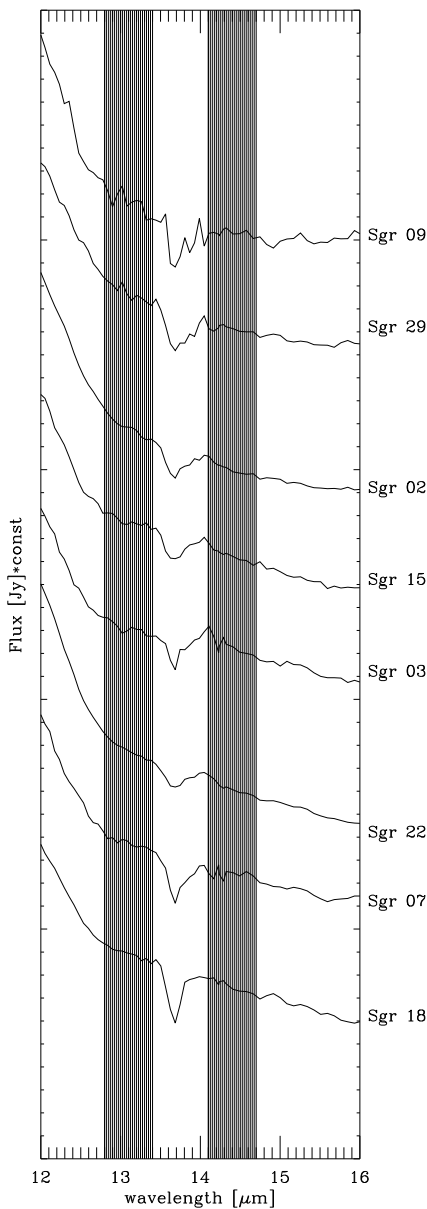


Figure 5. Spitzer spectra around $13.7\mu\text{m}$ of the observed stars, showing the C_2H_2 absorption. The two grey bands represent the continuum used to measure the band strengths.

9 DISCUSSION

9.1 Estimating metallicities

The survey of carbon-rich AGB stars in the Local Group has yielded *Spitzer* IRS spectra of a large sample of stars in galaxies covering a range of metallicities.

The metallicity of extragalactic AGB stars is normally taken

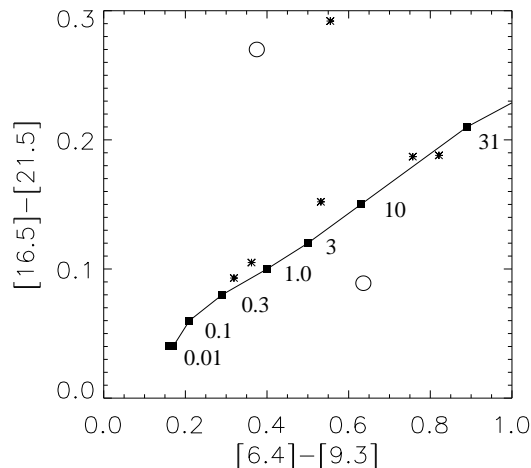


Figure 6. $[16.5] - [21.5]$ vs. $[6.4] - [9.3]$ colour diagram. Asterisks and open circles represent the stars we observed. The solid line and filled squares represent a series of *DUSTY* models, as described by Zijlstra et al. (2006a). The optical depth at $1\mu\text{m}$ is indicated for each model

as that of the underlying dominant stellar population of the galaxy. Individual metallicities of carbon stars are especially difficult to determine. Generally, stellar metallicities are determined from the strengths of fine-structure lines from heavy elements in optical or near-infrared spectra. The continua of AGB stars are very uncertain, due to the presence of multiple, overlapping molecular bands in their envelopes, e.g. CO and CN. To model this continuum, a hydrostatic stellar atmosphere model is required, with a known surface gravity, C/O abundance ratio, and effective temperature. Such models have been made to determine the metallicity of Local Group AGB stars, but are very time-consuming, and have been applied to only a small number of stars (de Laverny et al. 2006).

The SiC feature is expected to depend on metallicity, through the Si abundance. It may be possible to use the strength of this feature in our *Spitzer* spectra to estimate the metallicity of the stars in our sample. Simultaneously, the C_2H_2 abundance depends on the amount of free carbon, $[(\text{C}-\text{O})/\text{O}]$ (Lagadec & Zijlstra 2008), which is expected to increase (on average) with decreasing metallicity (e.g. Matsuura et al. 2005). Thus the *Spitzer* spectra provide two means of determining metallicity.

Fig. 11 shows the equivalent width of the C_2H_2 $7.5\mu\text{m}$ feature versus the SiC flux-over-continuum ratio, for all the Local Group carbon stars we observed. A clear separation is seen between the stars from different galaxies, i.e. different metallicities. The Galactic stars, which are expected to be the most metal-rich, have the largest SiC/C ratio for a given C_2H_2 $7.5\mu\text{m}$ equivalent width. The LMC stars are spread out between the SMC and Galactic stars. The diagram shows a good (average) separation between the galaxies, in order of expected metallicity. Stars from each individual galaxy show a significant spread, which may be due to a spread in metallicity within a galaxy, or due to an evolutionary spread, as the stars will show an increasing carbon dredge-up over time. But for the full carbon-star population, this diagram appears to provide a metallicity indicator.

We can apply this diagram to the stars observed in this paper. The two galactic foreground stars fall within the general population of Galactic stars, with one star (Sgr 22) showing an unusually high SiC/C ratio which can be interpreted as arising from a high metal-

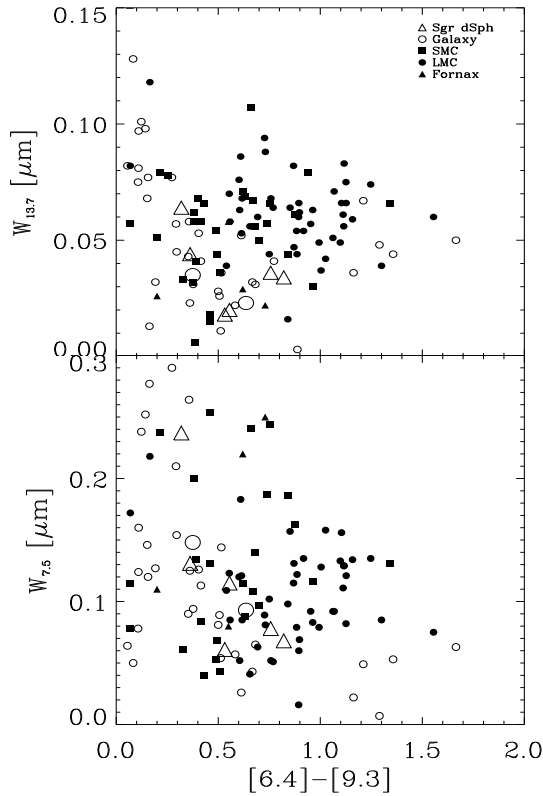


Figure 7. The equivalent width of the C_2H_2 features at $13.7\mu m$ (upper panel) and $7.5\mu m$ (lower panel) as a function of $[6.4]-[9.3]$ colour. The plot combines stars from the present sample and stars from previous Local Group observations: open triangles represent the current Sgr dSph sample, filled squares the SMC stars from Sloan et al. (2006) and Lagadec et al. (2007) samples, open circles the ISO Galactic sample defined by Sloan et al. (2006), filled circles the LMC sample of Zijlstra et al. (2006b) and Leisenring et al. (2008), and triangles stars from the Matsuura et al. (2007) Fornax sample.

licity. Surprisingly, the stars in the Sgr dSph are found between the Galactic and LMC stars, with an indicated metallicity higher than that of the LMC, although still sub-solar. Based on this diagram, the observed Sgr dSph carbon stars are the most metal-rich population after the Galactic stars.

9.2 Metal-rich carbon stars in the Sgr dSph

The dominant giant branch population in the Sgr dSph is believed to have a metallicity ($[Fe/H]$) ~ -0.55 or less (Whitelock et al. 1996, Dudziak et al. 2000, Carraro et al. 2007) which is lower than that of the LMC. The observed high metallicity implied for the dusty carbon stars in our Sgr dSph sample is therefore unexpected.

Evidence for a more metal-rich stellar population in the Sgr dSph was first detected by Bonifacio et al. (2004), who, based on spectroscopy of ten giants, found the dominant population to have $[Fe/H] = -0.25$, much higher than what is found from typical AGB stars. Zijlstra et al. (2006a) and Kniazev et al. (2008) show that one of the four planetary nebulae in the galaxy has the same high metallicity, confirming the existence of this population even if it does not dominate. Chou et al. (2007) find a median metallicity

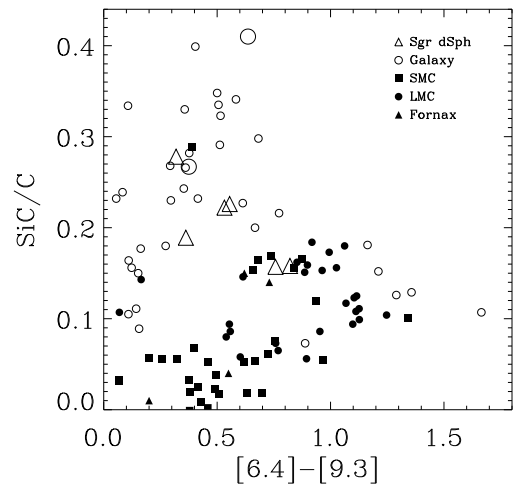


Figure 8. The strength of the SiC features as a function of the $[6.4]-[9.3]$ colour. $L/C(SiC)$ is the integrated-flux-to-continuum ratio of the SiC feature (Sec. 5). Comparison data are from the literature are as in Fig.7

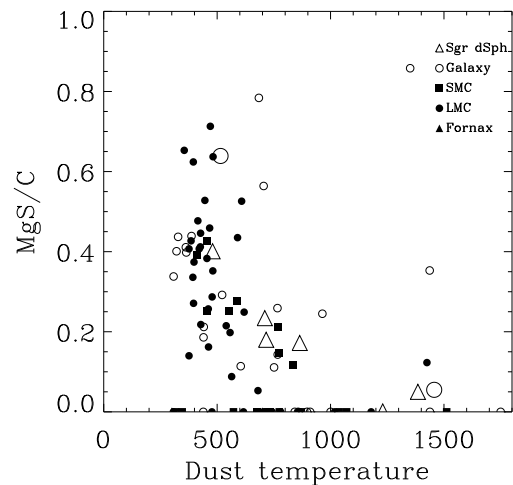


Figure 9. Strength of the MgS feature as a function of dust temperature estimated from the $[16.5]-[21.5]$ colour. Literature data as in Fig.7

in the core of the Sgr dSph of $[Fe/H] = -0.4$, similar to the LMC and again a little higher than typical AGB stars.

The dusty carbon stars studied in this paper appear to be comparatively metal-rich. It is therefore natural to suggest that they could be an AGB counterpart of the population whose age has been estimated at 1 Gyr (Bonifacio et al. 2004), the formation of which may have been triggered by the passage of the dwarf galaxy through the Galactic disc. However, their pulsation periods, which range from 310 to 512 days, imply considerably older ages. For example there are three carbon Miras which have periods around 490 days (Nishida et al. 2000) in Magellanic Cloud Clusters which have ages about 1.6 Gyr (Mucciarelli et al. 2007a,b; Glatt et al. 2008), whilst van Loon et al. (2003) suggest that the cluster KMHK 1603, which contains a carbon-rich Mira with a period of 680 days, has an age of 0.9-1.0 Gyr. The kinematics of Galactic carbon-rich Miras (Feast et

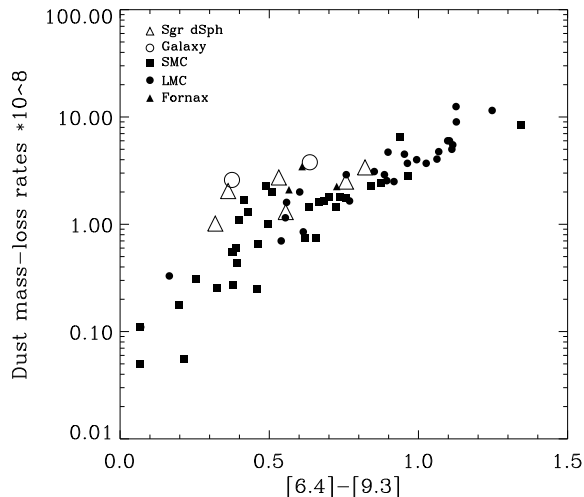


Figure 10. Dust mass-loss rates as a function of the $[6.4]–[9.3]$ colour. The comparison data are described in Fig. 7

al. 2006) is also consistent with increasing periods going with decreasing age. The periods of the Sgr dSph Miras would therefore imply ages of 2 to 3 Gyr, or perhaps a little greater. More work is required to reconcile these observations.

One can wonder why a relatively small galaxy would show the most metal-rich stellar population in the Local Group after the two main spirals (e.g. Zijlstra et al. 2006a). In general the dwarf spheroidals show a much steeper age-metallicity relation than do dwarf irregulars of the same luminosity. Dwarf spheroidals are found around large galaxies while the dwarf irregulars are more isolated systems, showing the effect of environment on enrichment history. It is also of interest that of the satellites of the Milky Way, only the Sgr dSph has reached such high metallicity. Fornax, otherwise a very similar system, contains carbon stars with more metal-poor characteristics (Matsuura et al. 2007). As the Sgr dSph is the nearest of the satellites (Fornax is around 130 kpc away), the effects of the Galaxy seem important.

There are two possible explanations for the very high metallicities. First, the stripping of the interstellar gas by a passage through the Milky Way may have allowed fast chemical evolution through stellar mass loss and supernovae. Second, the system may have captured gas from the Milky Way. The second option may have some support from the fact that the high metallicity is the same as that of the Galactic disk at the orbital distance of the Sgr dSph.

9.3 Two foreground carbon stars

As discussed in Sec. 3.3, two stars in our sample, Sgr 02 and Sgr 22, belong to the Milky Way Galaxy while the other stars are members of the Sgr dSph. These stars have been selected through their J and K colours and were not spectroscopically confirmed carbon stars before these observations. The *Spitzer* spectra clearly show that these stars are carbon-rich AGB stars. Their distance is estimated to be 17.1 kpc and 16.0 kpc for Sgr 02 and Sgr 22, respectively, from their infrared colours (see Sec. 7). Sgr 22 displays the strongest SiC feature among all the stars from our present Local Group sample (including the Galaxy). The other foreground star, Sgr 02, has a weaker SiC feature than Sgr 22, but Fig. 8 indicates

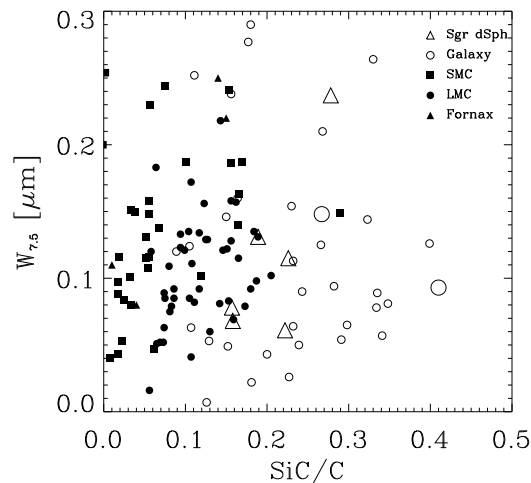


Figure 11. Strength of the C_2H_2 $7.5\mu m$ feature as function of the strength of the SiC feature. The comparison data are as described in Fig. 7

that its SiC feature strength is similar to the ones observed in the Galaxy rather than in more metal-poor galaxies.

The two Galactic stars are on line of sight to the Sgr dSph, and they are located on the far side of the Galaxy, close to the solar circle. There are very few carbon stars known in the inner Galaxy: carbon star distribution begins around the solar circle and extends outwards (Le Bertre et al. 2001). The two stars are therefore located around the inner edge of the carbon star distribution and should be similar to carbon stars in the Solar neighbourhood. However, their height above the Galactic plane is 3.6 and 4.9 kpc respectively. This is well beyond what is expected from the disc stars. There is no clear explanation, and it would be very interesting to establish the metallicity of other halo carbon stars, some of which are known to be Mira variables (e.g. Totten et al. 2000; Mauron 2008). The high metallicity suggests the stars escaped from the disc. Whether the escape process was triggered by the Sgr dSph passage is not clear.

10 CONCLUSIONS

We have presented a *Spitzer* spectroscopic survey of six carbon-rich AGB stars in Sgr dSph and two serendipitously discovered Galactic carbon stars. We used the low-resolution short-low and long-low mode of the IRS spectrometer to obtain mid-infrared spectra covering the range $5–38\mu m$. These observations enabled us to study dust and gas features from the circumstellar envelopes around these stars. We observed molecular absorption bands due to C_2H_2 at 7.5 and $13.7\mu m$. A weak absorption feature at $14.3\mu m$, due to HCN, is observed in two stars. A weak absorption feature at $5.8\mu m$ due to a carbonyl group (X-CO) is observed around two stars and might be present in the spectra of three others. The continuum of all the observed stars is due to emission from amorphous carbon, which does not display any spectral features. All the stars show a SiC feature at $11.3\mu m$. A broad dust emission emission due to MgS is also observed for six of the stars around $30\mu m$.

Radial velocity measurements show that two of our sample are actually carbon stars. The remaining six stars in our sample are members, as confirmed with radial velocities, infrared colour-magnitude relations, and/or period-luminosity relations. One of the

two Galactic carbon stars displays the strongest SiC feature ever observed. Both Galactic stars are certainly carbon stars located at the far side of the solar circle, but they have unexpectedly large distances from the Galactic plane.

We fitted the SEDs of all the observed spectra using the radiative transfer code DUSTY. The estimated dust mass-loss rates are found to be in the range $1.0\text{--}3.3 \times 10^{-8} M_{\odot} \text{yr}^{-1}$.

The observed strengths of C_2H_2 and SiC are very similar to the ones observed for Galactic carbon stars. Stronger C_2H_2 and weaker SiC feature were expected in this metal-poor dwarf galaxy. We have shown that the strength of these features depends on the metallicity and that the observed stars have metallicities close to Galactic values. This result is unexpected, as the usual measurements of the metallicity ($[\text{Fe}/\text{H}]$) of the Sgr dSph range from -0.4 to -0.7 . The enhanced metallicity of the observed carbon stars indicates that the interstellar medium in the Sgr dSph has been strongly enriched.

ACKNOWLEDGMENTS

EL acknowledges support from a STFC rolling grant. EL thanks Xander Tielens and Kevin Volk for very helpful discussions during the preparation of this paper. These observations were made with the *Spitzer Space Telescope*, which is operated by JPL, California Institute of Technology under NASA contract 1407. This research has made use of the SIMBAD and VIZIER databases, operated at the Centre de Données astronomiques de Strasbourg, and the Infrared Science Archive at the Infrared Processing and Analysis Center, which is operated by JPL.

REFERENCES

- Bellazzini M., Correnti M., Ferraro F. R., Monaco L., & Montegriffo P. 2006, *A&A*, 446, L1
- Bowen G. H., Willson L. A., 1991, *ApJL*, 375, L53
- Bonifacio P., Sbordone L., Marconi G., Pasquini L., & Hill V. 2004, *A&A*, 414, 503
- Carraro G., Zinn R., & Moni Bidin C. 2007, *A&A*, 466, 181
- Chou M.-Y., et al. 2007, *ApJ*, 670, 346
- de Laverny P., Abia C., Domínguez I., Plez B., Straniero O., Wahlin R., Eriksson K., & Jørgensen U. G. 2006, *A&A*, 446, 1107
- Dray L. M., Tout C. A., Karakas A. I., Lattanzio J. C., 2003, *MNRAS*, 338, 973
- Dudziak G., Péquignot D., Zijlstra A. A., & Walsh J. R. 2000, *A&A*, 363, 717
- Feast M. W., Whitelock P. A., Menzies J. W., *MNRAS*, 2006, 369, 791
- Gehrz R. 1989, *Interstellar Dust*, 135, 445
- Glatt K., et al., 2008, *AJ*, 136, 1703
- Groenewegen M. A. T., et al., 2007, *MNRAS*, 376, 313
- Hanner M. 1988, *Infrared Observations of Comets Halley and Wilson and Properties of the Grains*, 22
- Hony S., Waters L. B. F. M., & Tielens A. G. G. M. 2002, *A&A*, 390, 533
- Houck J. R., et al., 2004, *ApJS*, 154, 18
- Ibata R. A., Wyse R. F. G., Gilmore G., Irwin M. J., & Suntzeff N. B. 1997, *AJ*, 113, 634
- Ivezic Z., Nenkova M., & Elitzur M., User manual for DUSTY, University of Kentucky internal report
- Kniazev A. Y., et al. 2008, *MNRAS*, 388, 1667
- Lagadec E., et al. 2007a, *MNRAS*, 376, 1270
- Lagadec E., Zijlstra, A. A., Matsuura, M., Menzies, J. W., van Loon, J. T., & Whitelock, P. A. 2008, *MNRAS*, 383, 399
- Lagadec E., & Zijlstra, A. A. 2008, *MNRAS*, 390, L59
- Le Bertre T., Matsuura M., Winters J. M., Murakami H., Yamamura I., Freund M., & Tanaka M. 2001, *A&A*, 376, 997
- Leisenring J. M., Kemper F., & Sloan G. C. 2008, *ApJ*, 681, 1557
- Loidl R., Lançon A., & Jørgensen U. G. 2001, *A&A*, 371, 1065
- Maeder A., 1992, *A&A*, 264, 105
- Mateo M., Kubiak M., Szymanski M., Kaluzny J., Krzeminski W., & Udalski A. 1995, *AJ*, 110, 1141
- Mathis J. S., Rumpl W., & Nordsieck K. H. 1977, *ApJ*, 217, 425
- Matsuura M., Zijlstra A. A., van Loon J. T., Yamamura I., Markwick A. J., Woods P. M., & Waters L. B. F. M. 2002, *ApJL*, 580, L133
- Matsuura M., et al. 2005, *A&A*, 434, 691
- Matsuura M., et al., 2006, *MNRAS*, 371, 415
- Matsuura M., et al. 2007, *MNRAS*, 382, 1889
- Mattsson L., Wahlin R., Höfner S., & Eriksson K. 2008, *A&A*, 484, L5
- Mauron N., 2008, *A&A*, 482, 151
- Mucciarelli A., Ferraro F. R., Origlia L., Fusi Pecci F., 2007a, *AJ*, 133, 2053
- Mucciarelli A., Origlia L., Ferraro F. R., 2007b, *AJ*, 134, 1813
- Nishida S., Tanabé T., Nakada Y., Matsumoto S., Sekiguchi K., Glass I. S., 2000, *MNRAS*, 313, 136
- Pégourié B. 1988, *A&A*, 194, 335
- Schlegel D. J., Finkbeiner D. P., & Davis, M. 1998, *ApJ*, 500, 525
- Sloan G. C., Kraemer, K. E., Matsuura M., Wood P. R., Price S. D., Egan M. P., 2006, *ApJ*, 645, 1118
- Sloan G. C., Kraemer K. E., Wood P. R., Zijlstra A. A., Bernard-Salas J., Devost D., & Houck J. R. 2008, *ApJ*, 686, 1056
- Speck A., Thompson G. D., Hofmeister A., 2005, *ApJ*, 634, 426
- Totten E. J., Irwin M. J., Whitelock P. A., 2000, *MNRAS*, 314, 630
- van Loon J. Th., Marshall J. R., Matsuura M., Zijlstra A. A., 2003, *MNRAS*, 341, 1205
- Volk K., Kwok S., & Hrivnak B. J. 1999, *ApJL*, 516, L99
- Volk K., Kwok S., Hrivnak B. J., & Szczerba R. 2002, *ApJ*, 567, 412
- Wachter A., Winters J. M., Schröder K.-P., & Sedlmayr E. 2008, *A&A*, 486, 497
- Werner M. W., et al. 2004, *ApJS*, 154, 1
- Whitelock P. A., Irwin M., & Catchpole R. M. 1996, *New Astronomy*, 1, 57
- Whitelock P. A., Feast M. W., Marang F., & Groenewegen M. A. T. 2006, *MNRAS*, 369, 751
- Whitelock P. A., Menzies J. W., Feast M. W., Matsunaga N., Tanabé T., Ita Y., 2009, *MNRAS*, in press
- Zijlstra A. A., 2004, *MNRAS*, 348, L23
- Zijlstra A. A., et al. 2006b, *MNRAS*, 370, 1961
- Zijlstra A. A., Gesicki K., Walsh J. R., Péquignot D., van Hoof P. A. M., Minniti D. 2006a, *MNRAS*, 369, 875